

SPECTRAL ELEMENT DISCONTINUOUS GALERKIN SIMULATIONS FOR WAKE POTENTIAL CALCULATIONS: NEKCEM*

Misun Min,^{†‡} Paul F. Fischer,[‡] Yong-Chul Chae,[§]

[‡]Mathematics and Computer Science, Argonne National Laboratory, Argonne, IL 60439, USA

[§]Advanced Photon Source, Argonne National Laboratory, Argonne, IL 60439, USA

Abstract

In this paper we present high-order spectral element discontinuous Galerkin simulations for wake field and wake potential calculations. Numerical discretizations are based on body-conforming hexagonal meshes on Gauss-Lobatto-Legendre grids. We demonstrate wake potential profiles for cylindrically symmetric cavity structures in 3D, including the cases for linear and quadratic transitions between two cross sections. Wake potential calculations are carried out on 2D surfaces for various bunch sizes.

INTRODUCTION

We have developed a large-scale computational code, NEKCEM [5], for computing wake fields and wake potentials [1, 2] in 3D structures. NEKCEM employs a high-order numerical scheme, namely, the spectral element discontinuous Galerkin method [3, 4]. It features accurate and efficient computations with high performance in parallel.

FORMULATIONS

In this section we present the governing equations to study beam dynamics and numerical discretizations in space and time. Formulations are used in a mixed form with Cartesian and cylindrical coordinates for the sake of convenience.

Maxwell's Equations

We begin with the Maxwell equations:

$$\mu \frac{\partial H}{\partial t} = -\nabla \times E, \quad \epsilon \frac{\partial E}{\partial t} = \nabla \times H - J \quad (1)$$

$$\nabla \cdot E = \frac{\rho}{\epsilon}, \quad \nabla \cdot H = 0, \quad (2)$$

where the current source J is defined for an on-axis Gaussian beam moving in the z -direction:

$$J = ce_z \rho(r) \rho(z - ct), \quad \rho(z) = \frac{1}{\sigma_z \sqrt{2\pi}} e^{-\frac{z^2}{2\sigma_z^2}}. \quad (3)$$

*Work supported by the U.S. Dept. of Energy under Contract DE-AC02-06CH11357.

[†]mmin@mcs.anl.gov

Conservation Form

We rewrite equation (1) into a conservation form

$$Q \frac{\partial q}{\partial t} + \nabla \cdot F(q) = 0 \quad (4)$$

by defining

$$q = (H_x, H_y, H_z, E_x, E_y, E_z)^T \quad (5)$$

$$Q = \text{diag}(\mu, \mu, \mu, \epsilon, \epsilon, \epsilon). \quad (6)$$

The flux $F(q)$ has the following form.

$$\begin{bmatrix} 0 & E_z & -E_y & 0 & -H_z & H_y \\ -E_z & 0 & E_x & H_z & 0 & -H_x \\ E_y & -E_x & 0 & -H_y & H_x & 0 \end{bmatrix}^T \quad (7)$$

Numerical Discretizations

We approximate solutions to Maxwell's equations in the computational domain Ω as a set of body-conforming, nonoverlapping hexagonal meshes Ω^e . We define a local solution \mathbf{q}_N on each Ω^e as

$$\mathbf{q}_N(x, t) = \sum_{j=0}^N q_j(t) L_j(x), \quad (8)$$

where $q_j(t)$ is the solution at N grid points x_j on Ω^e , and $L_j(x)$ is the three-dimensional Legendre Lagrange interpolation polynomial associated with the N -nodes [3]. We seek the local solutions \mathbf{q}_N

$$\left(Q \frac{\partial \mathbf{q}_N}{\partial t} + \nabla \cdot F(\mathbf{q}_N), \phi \right)_{\Omega^e} = (\hat{n} \cdot [F - F^*], \phi)_{\partial \Omega^e}, \quad (9)$$

where the local discontinuous test function is $\phi = L_i(x)$ and the numerical fluxes F^* are defined as in [4].

We use the fourth-order Runge-Kutta method for time integration.

Initial Conditions

To describe the electromagnetic fields at the presence of the Gaussian beam for the initial time step, we first solve the Poisson equation in two dimensions at the cross section of the initial beam position

$$\nabla^2 \Phi^{2D}(r) = -\frac{\rho^{2D}(r)}{\epsilon} \quad (10)$$

and get the two-dimensional electric field at the cross section

$$E^{2D} = -\nabla\Phi^{2D}(r). \quad (11)$$

Then, we assign an initial electric field E in three dimensions along the z -direction, using the two-dimensional electric field E^{2D} scaled by the initial Gaussian distribution $\rho(z)$ as

$$E(r, z) = E^{2D}(r)\rho(z). \quad (12)$$

Boundary Conditions

We apply the uniaxial perfectly matched layer (UPML) [6] in the z -direction and the perfectly electric conducting (PEC) boundary [4] in the radial direction.

UPML formulations in 3D are defined as follows:

$$\frac{\partial H_z}{\partial y} - \frac{\partial H_y}{\partial z} = \frac{\partial D_x}{\partial t} + \frac{1}{\epsilon}\sigma_y D_x \quad (13)$$

$$\frac{\partial H_x}{\partial z} - \frac{\partial H_z}{\partial x} = \frac{\partial D_y}{\partial t} + \frac{1}{\epsilon}\sigma_z D_y \quad (14)$$

$$\frac{\partial H_y}{\partial x} - \frac{\partial H_x}{\partial y} = \frac{\partial D_z}{\partial t} + \frac{1}{\epsilon}\sigma_x D_z, \quad (15)$$

where $\sigma_x = -(x/d)^m(m+1)\ln(R)/2\eta d$, denoting d , x , m , R , and η for PML size, PML depth, polynomial grading, reflection error, and impedance, respectively. In UPML, the components of E are updated by

$$\epsilon \left[\frac{\partial E_x}{\partial t} + \frac{\sigma_z}{\epsilon} E_x \right] = \frac{\partial D_x}{\partial t} + \frac{\sigma_x}{\epsilon} D_x \quad (16)$$

$$\epsilon \left[\frac{\partial E_y}{\partial t} + \frac{\sigma_x}{\epsilon} E_y \right] = \frac{\partial D_y}{\partial t} + \frac{\sigma_y}{\epsilon} D_y \quad (17)$$

$$\epsilon \left[\frac{\partial E_z}{\partial t} + \frac{\sigma_y}{\epsilon} E_z \right] = \frac{\partial D_z}{\partial t} + \frac{\sigma_z}{\epsilon} D_z. \quad (18)$$

A similar formula is used in UPML to update the components of H . In our simulations we apply UPML only in the x -direction by choosing $\sigma_y = \sigma_z = 0$.

PEC boundary conditions are assigned at the boundaries in the radial direction satisfying

$$\hat{n} \times E = \hat{n} \cdot H = 0. \quad (19)$$

COMPUTATIONAL RESULTS

We show the performance of NEKCEM and demonstrate the wake potential profiles for beam dynamics on various cavity structures.

Performance

To demonstrate the performance of NEKCEM, we compute the case with standing wave solutions for the Maxwell's equations with periodic boundaries on a cube mesh. Computations are performed with 32 processors on the Linux cluster "Jazz" at Argonne for various computational sizes by increasing the number of elements and the degree of the polynomials. Figure 1 plots CPU time vs.

degree of freedom and errors vs. degree of freedom for different degrees of polynomials. The figure shows that CPU time increases linearly depending on the degree of freedom but is not dominated by the increases in the degree of the polynomials. Errors are much smaller with a higher degree of polynomial for a fixed number of grids. This result implies that one can obtain better efficiency and accuracy with the high-order method presented in this paper.

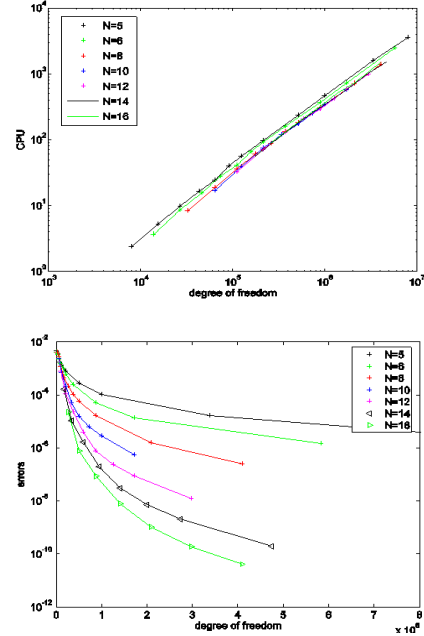


Figure 1: Performance with 32 processors on the Argonne Linux cluster "Jazz"; showing CPU time vs. degree of freedom (top) and errors in log scale vs. degree of freedom (bottom).

Wake Potentials

Figure 2 shows the electric field amplitude using contour lines on a half side of a pillbox mesh with circle cross-section radius $r = 1$ and $r = 2$ for bunch size $\sigma_z = 1.0$. The wake potential calculations are carried out on the 2D surface at $r = 1$ for different bunch sizes, $\sigma_z = 0.25, 0.5, 0.75, 1.0$, with a fixed $\sigma_r = 0.1$, which show good agreement with ABCI results. Figure 3 shows meshes for the cavities with linear and quadratic transitions between circle cross sections with radius changes from $r = 1$ to $r = 2$. Figure 4 shows wake potential calculations carried out on the 2D surface at $r = 1$ for different bunch sizes with a fixed $\sigma_r = 0.1$ on the meshes shown in Figure 3. Wake potentials with linear and quadratic transitions show reasonable profiles corresponding to the changes of the bunch sizes $\sigma_z = 0.25, 0.5, 0.75, 1.0$.

CONCLUSIONS

We have applied the spectral element discontinuous Galerkin method to beam simulations for three-

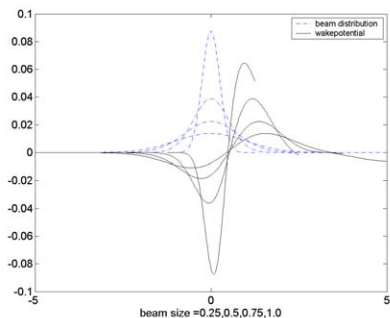
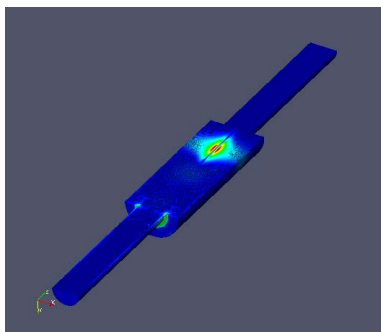


Figure 2: Contour lines of the electric field in amplitude on a half side of a pillbox mesh with circle cross-section radius $r = 4$ and $r = 2$ (top). Wake potential on the surface at $r = 1$ for $\sigma_z = 0.25, 0.5, 0.75, 1.0$ and $\sigma_r = 0.1$ (bottom).

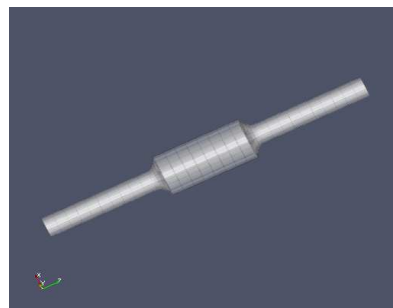
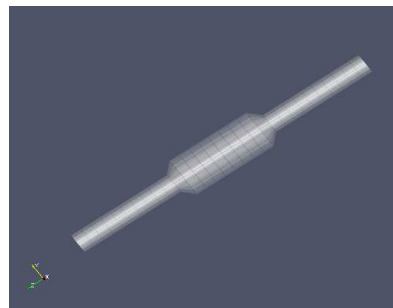


Figure 3: Meshes with circle cross sections with linear (top) and quadratic (bottom) transitions: tube radius is $r = 1$ for the outgoing tubes on sides.

dimensional cylindrical cavities with linear and quadratic transitions between circle cross sections. The wake potential calculations show resonable profiles depending on the bunch size. We are currently tracking a 1 ps beam moving through meter-scale cavities with linear and quadratic transitions between different sizes of elliptic cross sections. Rigorous comparisons on the wake potential calculations with other codes will be presented in a later paper.

REFERENCES

- [1] Y.C. Chae, "Horizontal Coupling Impedance of the APS Storage Ring," in Proc. 2003 PAC (2003), p. 3011.
- [2] Y.H. Chin, "User's Guide for ABCI Version 9.4 and Introducing the ABCI Windows Application Package," KEK Report (2005) 2005-06.
- [3] M.O. Deville, P.F. Fischer, and E.H. Mund, "High Order Methods for Incompressible Fluid Flow," Cambridge University Press (2002).
- [4] J.S. Hesthaven and T. Warburton, "Nodal High Order Methods on Unstructured Grids - I. Time-Domain Solution of Maxwell's Equations," J. Comp. Physics, 101 (2002), p. 186.
- [5] M.S. Min and P.F. Fischer, "NEKCEM," Mathematics and Computer Science Division, Argonne National Laboratory. <http://mercurial.mcs.anl.gov/nekcem/>.
- [6] A. Taflov and S.C. Hagness, "Computational Electromagnetics: The Finite-Difference Time Domain Method," Artech House, 3rd ed. (2005).

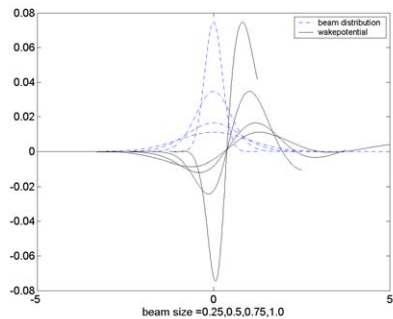
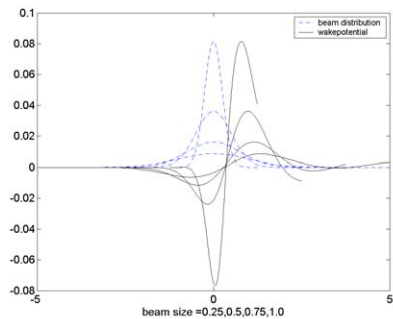


Figure 4: Wake potentials on the surface at $r = 1$ for $\sigma_z = 0.25, 0.5, 0.75, 1.0$ and $\sigma_r = 0.1$ on the meshes (shown in Figure 3) with linear (top) and quadratic (bottom) transitions.